Physics of Plasmas

RESEARCH ARTICLE | JANUARY 20 2022

Experimental observations of multiple modes of filamentary structures in the magnetized dusty plasma experiment (MDPX) device

EP FREE

S. Williams ; S. Chakraborty Thakur ; M. Menati ; E. Thomas, Jr.

Check for updates

Physics of Plasmas 29, 012110 (2022)
https://doi.org/10.1063/5.0065516
CHORUS

View Online
Export Citation
CrossMark

Articles You May Be Interested In

Predictions for Gyro-phase Drift in MDPX

Physics of Plasmas (October 2016)

The magnetized dusty plasma experiment (MDPX)

AIP Conference Proceedings (January 2018)

Experimental observation and numerical investigation of filamentary structures in magnetized plasmas

Physics of Plasmas (February 2020)

31 August 2023 11:57:18

AIP Publishing

Physics of Plasmas ARTICLE scitation.org/journal/php

Experimental observations of multiple modes of filamentary structures in the magnetized dusty plasma experiment (MDPX) device

Cite as: Phys. Plasmas **29**, 012110 (2022); doi: 10.1063/5.0065516
Submitted: 2 August 2021 · Accepted: 23 December 2021 ·
Published Online: 20 January 2022

View Online Export Citation CrossMark

S. Williams,[a] S. Chakraborty Thakur,[b] M. Menati,[b] and E. Thomas, Jr.[b]

AFFILIATIONS

Department of Physics, Auburn University, Auburn, Alabama 36832, USA

[a]Author to whom correspondence should be addressed: saw0051@auburn.edu
[b]Electronic addresses: szc0199@auburn.edu; mzm0085@auburn.edu; and etjr@auburn.edu

ABSTRACT

Due to the small charge-to-mass ratio of dust particles, it is often necessary to use large magnetic fields of $B \geq 1$ T, in order to observe the influence of magnetic forces in laboratory dusty plasmas. However, when experiments are performed at high magnetic fields in capacitively coupled, radio frequency discharges used for these dusty plasma experiments, the plasma is often observed to form filamentary structures between the electrodes that are aligned to the external magnetic field which disrupt the uniformity of the plasma and adversely impact some of our dusty plasma experiments. Recent experiments performed in the Magnetized Dusty Plasma Experiment device seek to identify and characterize these filamentary structures. This paper discusses the morphology of several distinct filamentary modes that are formed in low temperature argon plasmas. Three different spatial modes of filaments that appear to be strongly dependent on the magnetic field and neutral pressure are identified. There is strong evidence that each spatial mode has a threshold condition that is dependent on the ion Hall parameter. The criteria for the formation of the filaments are shown to be consistent with predictions of recent numerical simulations.

Published under an exclusive license by AIP Publishing. https://doi.org/10.1063/5.0065516

31 August 2023 11:57:18

I. INTRODUCTION

The physical properties of complex, or dusty plasmas, have been a topic of interest to the basic and low temperature plasma communities for several decades. To study the effect of magnetic fields on dusty plasmas, large magnetic fields ($B \geq 1$ T) are required.[1] However, these large magnetic fields can adversely impact the stability of the plasma, thus motivating complementary studies of the performance, stability, and pattern formation in the plasma itself. Moreover, because the formation of self-organized, strongly coupled structures is a signature feature of dusty plasma phenomena, as studies have begun to include the effects of magnetic fields, there has been a great deal of interest in understanding how pattern formation in both the background plasma and the dusty plasma is modified. However, as originally discussed in works by Konopka *et al.*,[2,3] and Schwabe *et al.*,[4] under certain conditions, the large magnetic field leads to the formation of nonuniform structures in the background plasma which disrupts the uniformity of the plasma and adversely impacts some of our dusty plasma experiments.

This nonuniformity, when viewed from the side (i.e., perpendicular to the magnetic field direction) as shown in Fig. 1, results in distinct, bright columns compared to the background plasma and aligned with the direction of the magnetic field. These columns are referred to as plasma filaments (the process is commonly referred to as filamentation) and are observed in the plasma, typically for $B \geq 0.5$ T. The history of documented individual filaments in highly magnetized plasmas is not very extensive. The first reported filaments of this phenomenon were in 2005 by Konopka *et al.*,[2,3] in which the authors report oblong and circular filaments found at 1.2 T.

When viewed from above, plasma filamentation has been observed to form various patterns within the plasma discharge.[5–9] These patterns include rings, spirals, large and small individual columns. Previous observations suggest the filamentation patterns is strongly connected to the geometry of the plasma chamber, notably the interelectrode gap, and the plasma parameters.[11] Furthermore, in Schwabe *et al.*,[4] it is shown that the dust particle behavior is substantially modified by the presence of filaments. While those past studies reported on the existence of filaments, there has been no additional effort to characterize the spatiotemporal features of the filaments. Understanding the conditions that lead to plasma filamentation and the impact of these large magnetic fields on capacitively coupled rf generated low temperature plasmas is the focus of this work.

Published under an exclusive license by AIP Publishing

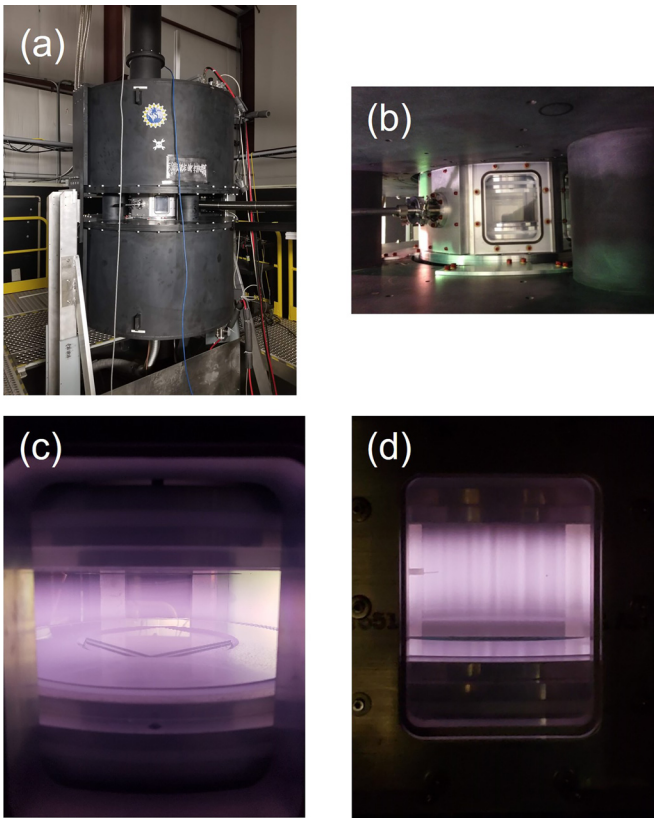

FIG. 1. Images of the Magnetized Dusty Plasma Experiment (MPDX) system, plasma chamber, and plasma discharges with and without a magnetic field. (a) View of the MPDX system showing the cryostat (painted black) that houses the four superconducting coils and the integrated vacuum chamber. (b) Closeup view of the vacuum chamber in the 50 cm diameter "warm bore" of the magnet. For the experiments reported here, the vacuum chamber uses a capacitively coupled plasma (CCP) configuration using an electrically floating upper electrode and powered lower electrode. (c) Argon glow discharge plasma with no magnetic field present. A Fluorine-doped Tin Oxide (FTO) glass plate that is placed on the bottom electrode is visible in this image. (d) Argon plasma glows discharge with a high magnetic field present. Filaments can be observed in the interelectrode gap (5 cm) between the upper and lower electrodes. A single tip Langmuir probe can be seen in this image (inserted into from the left).

This paper reports on studies performed using the Magnetized Dusty Plasma Experiment (MDPX) device, images of which are shown in Fig. 1.[10,11] Previously reported studies on the MDPX device have focused on the response of the dust component of the plasma to the large magnetic field, such as the melting of plasma crystals[12] and the discovery of a new type of imposed pattern formation.[13] In those previous studies, great care was taken to operate the MDPX device under conditions that minimized the formation of the plasma filaments. This work focuses on the formation and characterization of distinct filament morphologies that appear reproducibly in the plasma as a function of magnetic field and neutral pressure. We report on the results of two experiments that investigate the evolution of the filaments with varying magnetic field and neutral gas pressure while holding the input RF power fixed at 1 W and the electrode gap fixed at 5 cm. The first experiment will describe filament behavior through pressure variations while both power input and magnetic field strength are held constant. The second experiment discusses the evolution of filament behavior during continuous magnetic field discharges from 3.5 to 1 T or lower, while holding pressure and power input constant throughout. In both experiments, when viewed through a top port of the MDPX experiment, filaments take on distinct shapes that we qualitatively identify as type 1—circular, type 2—elongated, type 3—spiral.

The experiment results presented in this paper show good qualitative and quantitative agreement with simulations by Menati *et al.*[14,15] in terms of the occurrence of filaments as based upon characteristic plasma scale lengths. This work will also consider how the spatial dimensions of the filaments scale with magnetic field and how they scale with ion gyroradius.

The remainder of this paper is organized as follows: Sec. II will describe the experimental setup and Sec. III will discuss the experimental observations of the filaments. Section IV will provide an analysis of the filament morphologies and will make comparisons with recent numerical simulations. Finally, Sec. V. will provide a brief summary and concluding remarks.

II. EXPERIMENTAL SETUP

The experiments discussed in this paper are performed using the Magnetized Dusty Plasma Experiment (MDPX) device at Auburn University. The MDPX device is a unique, superconducting, multi-configuration, high magnetic field experimental facility that has been optimized for the study of dusty plasmas in strongly magnetized plasmas. The design and operation of the MDPX device has been discussed extensively in previous works[8,13–15] and only a brief summary of its key features, relevant to this investigation, are described below.

A. Hardware configuration

The MDPX device is composed of two primary components, a large cryostat that houses the magnetic field coils and the vacuum chamber where plasma experiments are performed. The cryostat has a cylindrical shape with an overall outer diameter of 122 cm and an axial length of 157 cm. The cryostat has a "split bore" configuration (as seen in Fig. 1), with a 19 cm gap between the upper and lower halves. The cryostat houses the four Nb:Ti superconducting coils, two in each half of the cryostat, that are used to generate the magnetic field. A 50 cm diameter warm bore at the center of the cryostat is where the vacuum chamber is placed. The use of the "split warm-bore" design ensures that there is both radial and axial access to the vacuum chamber.

In these studies, the "standard" MDPX octagonal vacuum chamber is used.[14] The vacuum chamber has a 45.7 cm outer diameter and a 35.6 cm inner diameter. In general, when plasmas are formed in the MDPX chamber, a capacitively coupled plasma (CCP) configuration is used with the plasma formed between a pair upper and lower aluminum electrodes that are 34.2 cm in diameter and separated by a gap of 5.0 cm. Plasmas are generated using a 13.56 MHz radio frequency (rf) generator operated between 1 and 10 W of input power. For these experiments, the top electrode is electrically floating and the bottom electrode is powered by the rf generator. The top cover of the vacuum chamber and the upper electrode both have circular "cutouts" to allow the plasma volume to be viewed from the top as shown in Fig. 2. The design and use of these cutouts for observing the plasma are described below, in Sec. II B.

31 August 2023 11:57:18

Published under an exclusive license by AIP Publishing

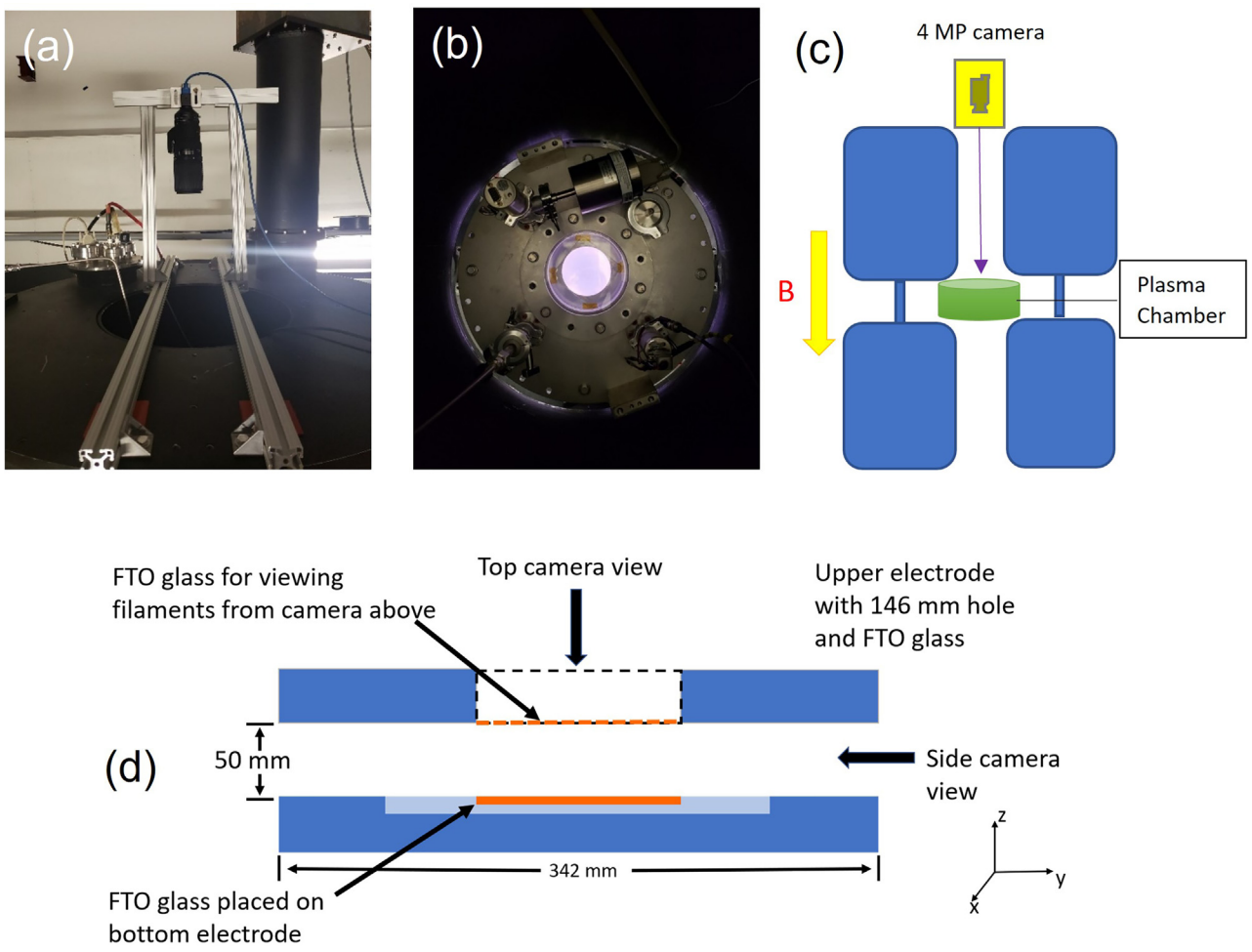

FIG. 2. (a) Picture of the Ximea xiQ MQ042MG-CM camera mounted above the magnet with a top–down view of the vacuum chamber. A 200 mm Nikon lens is attached to the Ximea to observe filaments clearly from the established camera placement. (b) View of argon plasma from above. The upper electrode contains a 14.6 cm diameter hole for viewing plasma. A square, FTO-coated glass plate is placed above the hole to maintain a uniform potential profile across the upper electrode. (c) A schematic drawing that shows the overall experimental configuration; and (d) a schematic drawing showing the MDPX octagonal vacuum chamber electrode configuration.

As compared to previously reported studies using the MDPX device, no dust particles are used or observed in these experiments. Argon plasmas are generated in the experiment at neutral gas pressures ranging from ∼3 to 7 Pa (22 to 53 mTorr) at magnetic fields ranging from a minimum of 0.5 T, where the filaments are first observed, up to 3.5 T.

In order to study the formation of filaments and their associated spatial structures, the experiment setup was configured to allow direct observation of the filaments through the top port of the MDPX vacuum chamber. This is accomplished by using a Ximea 4MP xiQ series camera to image the filaments created. The camera was placed on housing that fits on the top of the magnet and gives the ability to view the chamber from above through the bore of the magnet. A 200 mm Nikon macro lens was placed on the camera and focused to view the filaments specifically for the magnet discharge experiment. The Ximea camera was operated using the XIMEA *CamTool* software that is provided with the camera hardware. The software configuration includes options to adjust for region of interest (ROI), exposure, gain, bit-depth, frame rate, and bandwidth. Figure 2 shows: (a) a photograph of the top-view camera and its support assembly on the MDPX device; (b) a photograph of an argon plasma in the MDPX device as viewed through the top port of the vacuum chamber; (c) a schematic drawing that shows the overall experimental configuration; and (d) a schematic drawing showing the MDPX octagonal vacuum chamber electrode configuration.

B. Plasma observation and measurements

As discussed in the introduction, the filaments are self-generated plasma structures that are formed along the magnetic field. When viewed from above, these filaments can take on an extensive variety of shapes and patterns. Therefore, it is essential to have the appropriate

31 August 2023 11:57:18

Published under an exclusive license by AIP Publishing

diagnostic configuration that can properly observe the filaments and monitor the plasma. The top cover of the vacuum chamber has a 14 cm diameter circular cutout, where a Plexiglas viewport is used to view the plasma.

As shown in Fig. 2(d), a $10 \times 10 \times 0.3\,\text{cm}^3$ glass plate with the Fluorine-doped Tin Oxide (FTO) coated side is placed, conducting side facing the plasma, in a designated cutout in the top electrode. This allows uniformity in the potential profile created from the electrodes while allowing visibility into the plasma created from above. The top electrode remains electrically floating and the bottom electrode is powered for the duration of the experiments. The ions remain at room temperature because of neutral collisions, while the electron temperature is measured to be in the range of 2–4 eV.[8]

A second $10 \times 10 \times 0.3\,\text{cm}^3$ FTO glass plate is placed within the 15.24 cm diameter, 3.1 mm deep depression of the bottom electrode with the FTO-coated side facing downward, toward the electrode. While the uncoated side (i.e., the insulated side) faces upward toward the plasma and top electrode as shown in Fig. 1(c). The purpose of a second glass plate is to encourage charge accumulation to help the formation of the filament columns as described in the paper by Menati *et al.*[14]

III. OBSERVATIONS OF PLASMA FILAMENTS

In the absence of a magnetic field, plasmas in the MDPX device are visually uniform and fill the plasma volume between the electrodes as shown in Fig. 1(c). A photograph of an argon plasma at $B = 0$ T is shown. While plasma operations in MDPX at high magnetic fields ($B \geq 0.5$ T) can have stable plasma operations, under certain low RF power ($R_{RF} \leq 10$ W) and low neutral pressure ($p \leq 10$ Pa) operating conditions, filaments can appear. As shown in Fig. 1(d), an argon plasma at $B = 1$ T, $p = 3.5$ Pa, and $P_{RF} = 1$ W, forms a highly nonuniform plasma. Vertical filaments, aligned parallel to the background magnetic field, appear in the chamber as bright columns with darker gaps in-between individual filaments. The appearance of the filaments and their dependence on the operating conditions of MDPX are consistent with the observations first reported in the high magnetic field studies at the Max Planck Institute by Schwabe *et al.*[4]

The filaments begin to appear within the plasma with an applied magnetic field strength of approximately 0.5 T at low neutral pressure and low applied RF power combinations. For the observations discussed in this work, the power input was held fixed at 1 W and the pressure was varied over a range of $p = 3.4$ to 6.6 Pa (25 to 50 mTorr). When viewed from the side, the filament columns become more distinct as the magnetic field increases. This is consistent with observations of the filaments when viewed from above, where distinct shapes are observed to form at the terminating end of the filament column on the top electrode as shown in Fig. 3. In the experiments reported here, the top electrode is allowed to remain electrically floating; however, similar observations of filamentary structures are made if the electrode is grounded.

Figure 3 shows an example of the filament properties when viewed from the side, in Fig. 3(a), and from the top, in Fig. 3(b), for the same set of operating conditions ($B = 2$ T, $p = 3.5$ Pa, $P_{RF} = 1$ W). As seen in Fig. 3, the elongated filament columns are clearly visible when viewed from the side. But, when viewed from above, several different distinct types are identified: type 1: circular, type 2: elongated,

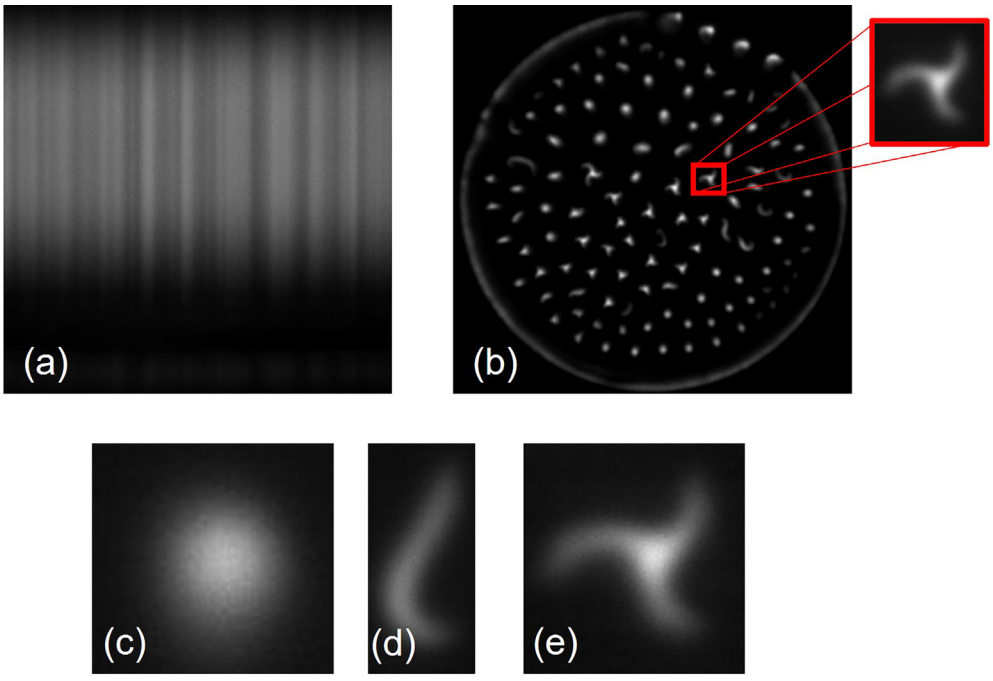

FIG. 3. Observations of plasma filaments in an argon plasma from (a) side and (b) above for the same operating parameters in MDPX: $B = 2$ T, $p = 3.5$ Pa, $P_{RF} = 1$ W. The inset in (b) shows a closeup of one of the spiral type filament morphologies. Over a range of experimental conditions, three distinct and reproducible filament "types" are identified: (c) type 1—circular, (d) type 2—elongated, and (e) type 3—spiral.

31 August 2023 11:57:18

Published under an exclusive license by AIP Publishing

and type 3: spiral. All three filament types are shown to co-exist in the plasma. The appearance of these different filament shapes is, of course, dependent on the magnetic field. However, the relative distribution of the different shapes also shows a strong response to changes in the input power and neutral gas pressure.

In the first experiment, we consider the variation in the filaments as a function of pressure. In this experiment, the RF power and magnetic field remain constant, but pressure is varied where it is observed that the distribution of filament types directly responds to the pressure change, as illustrated in Fig. 4. Here, top-view images of the filaments are shown for $B = 2$ T, $P_{RF} = 1$ W, and several different pressures. In Fig. 4(a), $p = 0.67$ Pa (5 mTorr), the initial formation of filaments is observed as the separation between brighter, lighter areas of plasma emission begin to coalesce and separate from the darker regions. At a pressure of $p = 1.6$ Pa (12 mTorr), as shown in Fig. 4(b), the filaments have begun to form with clear columns and appear very bright from above. As the pressure increases from 2.7 Pa (20 mTorr) to 4.4 Pa (33 mTorr), filaments begin to acquire a variety of shape patterns as indicated in Figs. 4(c)–4(e). With additional increases in the pressure, the number of distinct filament columns within the plasma decreases as shown in Fig. 4(f) at $p = 5.2$ Pa (40 mTorr) and Fig. 4(g) at $p = 6$ Pa (45 mTorr). At pressures $p > 6$ Pa, the number of discrete filaments continues to decrease to the point where none are visible in this configuration above $p = 6.6$ Pa. The authors note that while other

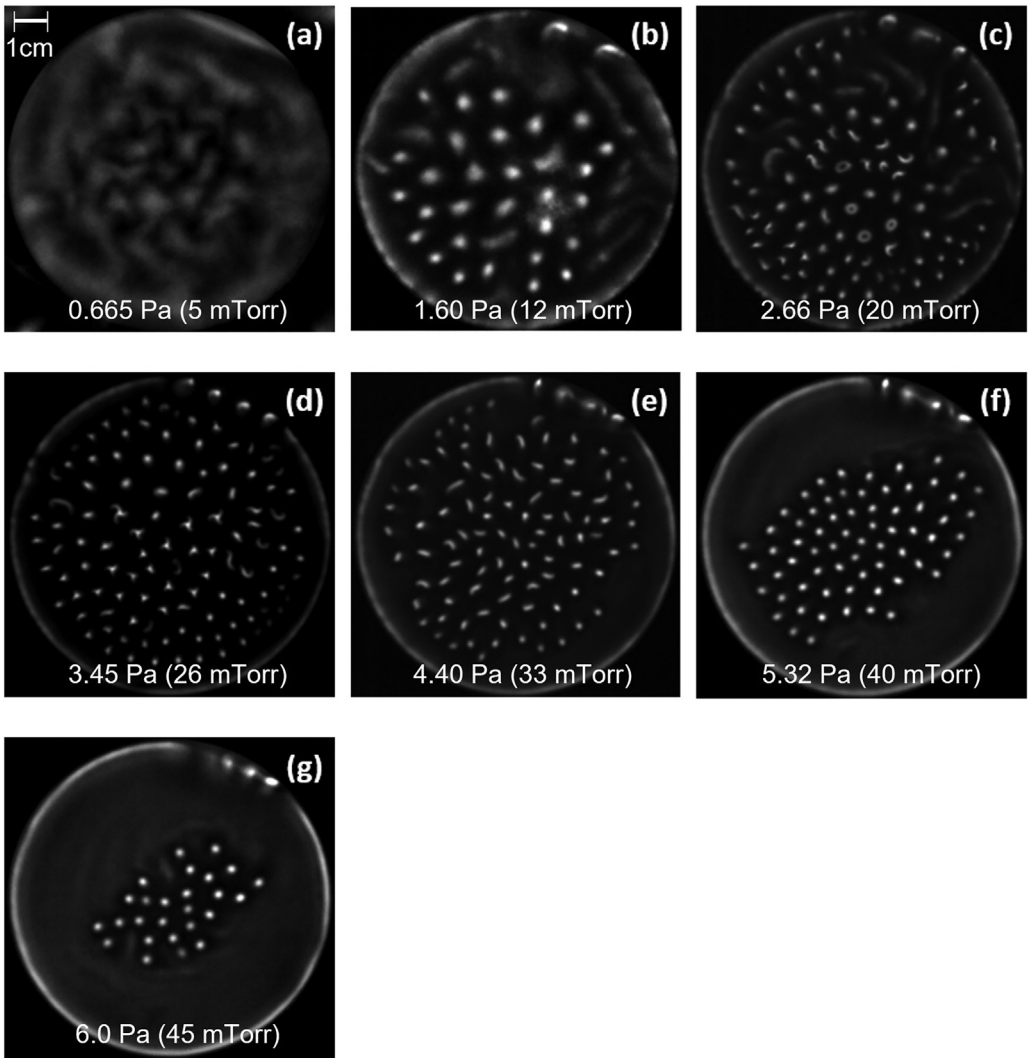

FIG. 4. Images of filaments from above with increasing pressure for a constant operating magnetic field of $B = 2$ T and applied RF power of $P_{RF} = 1$ W. Filaments begin to become distinct around 1.60 Pa (12 mTorr) and fill the volume of the observable area, peaking between 3.40 and 4.45 Pa (25–35 mTorr) with scale length reduction and clear boundaries. As pressure increases further, there is a reduction in the number of filaments that occupy the observable area. Additionally, with high pressure (around 5.3 Pa), type 1 filaments highly dominate the population. (a) 0.665 Pa (5 mTorr), (b) 1.60 Pa (12 mTorr), (c) 2.66 Pa (20 mTorr), (d) 3.45 Pa (26 mTorr), (e) 4.40 Pa (33 mTorr), (f) 5.32 Pa (40 mTorr), and (g) 6.0 Pa (45 mTorr).

31 August 2023 11:57:18

Published under an exclusive license by AIP Publishing

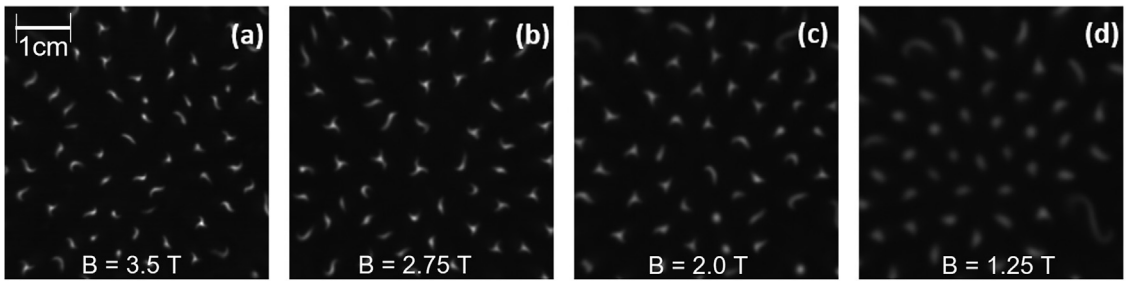

FIG. 5. Observations of plasma filaments as the magnetic field is decreased. Both power input and pressure remain constant during discharge (1 W and 3.45 Pa, respectively). At high magnetic field strength, filaments maintain relatively high light intensity, distinct boundaries, smaller area, and all three filament types are present. As field decreases, light intensity decreases, individual filament area increases, boundaries become less distinct, and some filament types are unobserved. At low field (1 T or less), only type 1 filaments are observed while their area increases over two times their area at high field (above 2.5 T). (a) 3.5, (b) 2.75, (c) 2.0, and (d) 1.25 T.

morphologies may be present, e.g., a circular structure observed in Fig. 4(c), the modes that will be analyzed are the most stable, robust, and repeatable filament structures that appear in the plasma.

In the second set of experiments, we consider the variation in the filaments as a function of magnetic field. In this study, an argon plasma is formed in the experiment at a constant pressure and RF power. The superconducting coils in the magnet are then allowed to discharge, leading to a controlled decrease in the magnetic field over a period of ~2 h from a peak of $B \geq 3$ T to zero. For each experimental case, the exact range of the magnetic field scan is dependent on the initial magnetic field at which the measurement process is started. Images are recorded using the Ximea camera at a rate of 1 Hz during the discharge process. This process is illustrated in Fig. 5 for an experiment with pressure, $p = 3.45$ Pa (26 mTorr), an input RF power, $P_{RF} = 1$ W, and a magnet discharge process that began at $B = 3.5$ T.

Similarly, to the first experiment, a variety of individual filament shapes are observed. Figure 5(a) shows the appearance of the filaments at $B = 3.5$ T. Here, the elongated (type 2) and spiral (type 3) are the dominant structures with circular (type 1) filaments virtually absent. In Fig. 5(b), at $B = 2.75$ T filaments appear larger in scale, spiral arms are more defined and elongated in comparison to 3.5 T, and the system remains dominated by elongated and spiral patterns. With a further decrease in the magnetic field, at $B = 2$ T in Fig. 5(c), filaments appear considerably less bright than the 3.5 T case, the size of filaments increases, and the number of circular (type 1) filaments has increased. Finally, in Fig. 5(d), where the magnetic field has decreased to $B = 1.25$ T, the filaments have clearly become less well-defined. The brightness of the filaments is significantly lower, the boundaries are less distinct, the size of the filaments has continued to increase, and the system becomes dominated by circular filaments while spirals are no longer present. The measurements shown in Fig. 5 were repeated for neutral pressures of $p = 4.4$, 5.3, and 6 Pa (33, 40, and 45 mTorr, respectively) with qualitatively similar results obtained for those cases as well.

For these studies, it is essential to be able to quantitatively classify the shape of the filament (i.e., type 1, 2, or 3) and the degree of filamentation (i.e., the area in pixels occupied by the filaments). To accomplish this, the public domain Java image processing program *FIJI* was used.[16] Images loaded into *FIJI* were processed via a thresholding step and then the "Analyze Particles" capability of *FIJI* is used to "tag" and identify the individual filaments. Using the shape descriptors of the particles, particularly the area, circularity, aspect ratio, and associated shape statistics, a Python program was developed that used the descriptor information to then classify the shape/type of the filament and the total area occupied by all of the filaments in a single image. This process is illustrated schematically in Fig. 6.

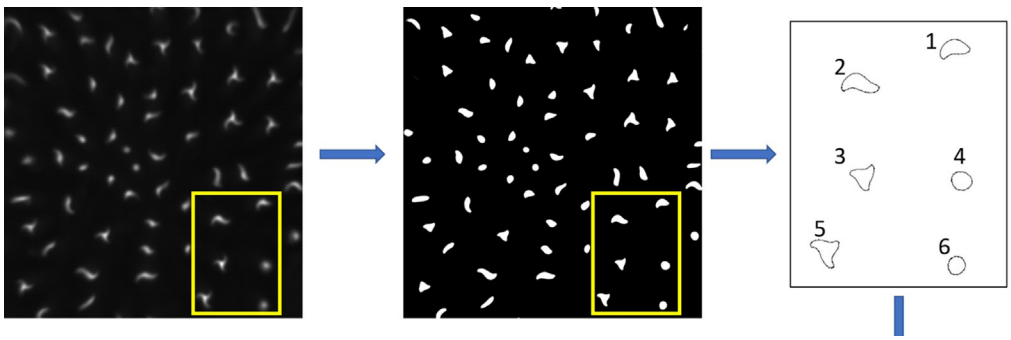

Filament	Type
1	2 (El)
2	2 (El)
3	3 (Sp)
4	1 (C)
5	3 (Sp)
6	1 (C)

FIG. 6. Sequence to illustrate the processing of images in order to obtain shape parameters and characterize the filament type. (a) Raw image of Ximea xiQ camera. (b) The image is then processed in the *FIJI* implementation of the *ImageJ* software framework, creating the "threshold" image (filaments white and background black). (c) Filaments within a region of interest are tracked and assigned shape parameters by *FIJI*; the output tables of these shape parameters are then processed using a Python code developed by our group to characterize the filaments into their different, types: 1 (C—circular), 2 (El—elongated), and 3 (Sp—spiral). For the region of interest shown in Figs. 6(a) and 6(b), the output table of identified filament types is shown to the right.

31 August 2023 11:57:18

Published under an exclusive license by AIP Publishing

Figure 7 shows the results of this analysis. The figures show the characterization of the filaments, by type, over a range from $B = 0.5$ to 3.5 T at a constant RF power of 1 W. Figure 7(a) shows measurements at $p = 3.5$ Pa (26 mTorr), Fig. 7(b) represents shows measurements at $p = 4.4$ Pa (33 mTorr) and Fig. 7(c) shows measurements at $p = 5.3$ Pa (40 mTorr). The data represents the number of filaments that are characterized as either a type 1, 2, or 3 by the Python code as a function of the magnetic field. Here, the plots show the evolution of the filament geometry as a function of magnetic field. The absence of data points below the turn-on threshold indicates that type of filament was not found at the correlated magnetic field. Moreover, beginning the discharge at higher magnetic fields (i.e., $B = 3.5$ T instead of $B = 3.0$ T) limits the allowable discharge time; therefore, increasing the minimum magnetic field from about $B = 0.75$ T to about $B = 1.25$ T, respectively.

The spiral shapes (type 3), appear in the plasma at the highest magnetic fields. By contrast, the circular (type 1) filaments appear at lower magnetic fields, $B \leq 2$ T. The type 2 filaments, at $p = 3.45$ Pa, appear in the plasma nearly universally at all magnetic fields, but at $p = 4.4$ Pa, these filaments appear at a magnetic field of around 1.5 T. Additionally, the color coding in Figs. 7(a)–7(c) corresponds to the three different filament types. As in Figs. 7(a) and 7(b), it shows the dominance of types 2 and 3 filaments at the higher magnetic fields and the type 1 filaments at the lower magnetic fields.

IV. ANALYSIS OF FILAMENT MORPHOLOGIES

The observations reported here indicate that the morphology and spatial distribution of the filaments are dependent on both the magnetic field and pressure. Therefore, it is important to consider a single analytic framework that will allow us to incorporate both effects. In recent numerical studies by Menati *et al.*[15] a three-dimensional fluid code is used to self-consistently study the properties of filaments and other self-organized plasma structures in strongly magnetized plasmas in the MDPX device. The simulation results indicate that there is a sensitive balance between the ion–neutral collision mean free path (λ_{mfp}, i.e., neutral pressure), ion gyroradius (ρ_i, i.e., magnetic field), and electron Debye length (λ_{De}, i.e., plasma density) that appears to determine whether filaments can appear in the plasma and suggests

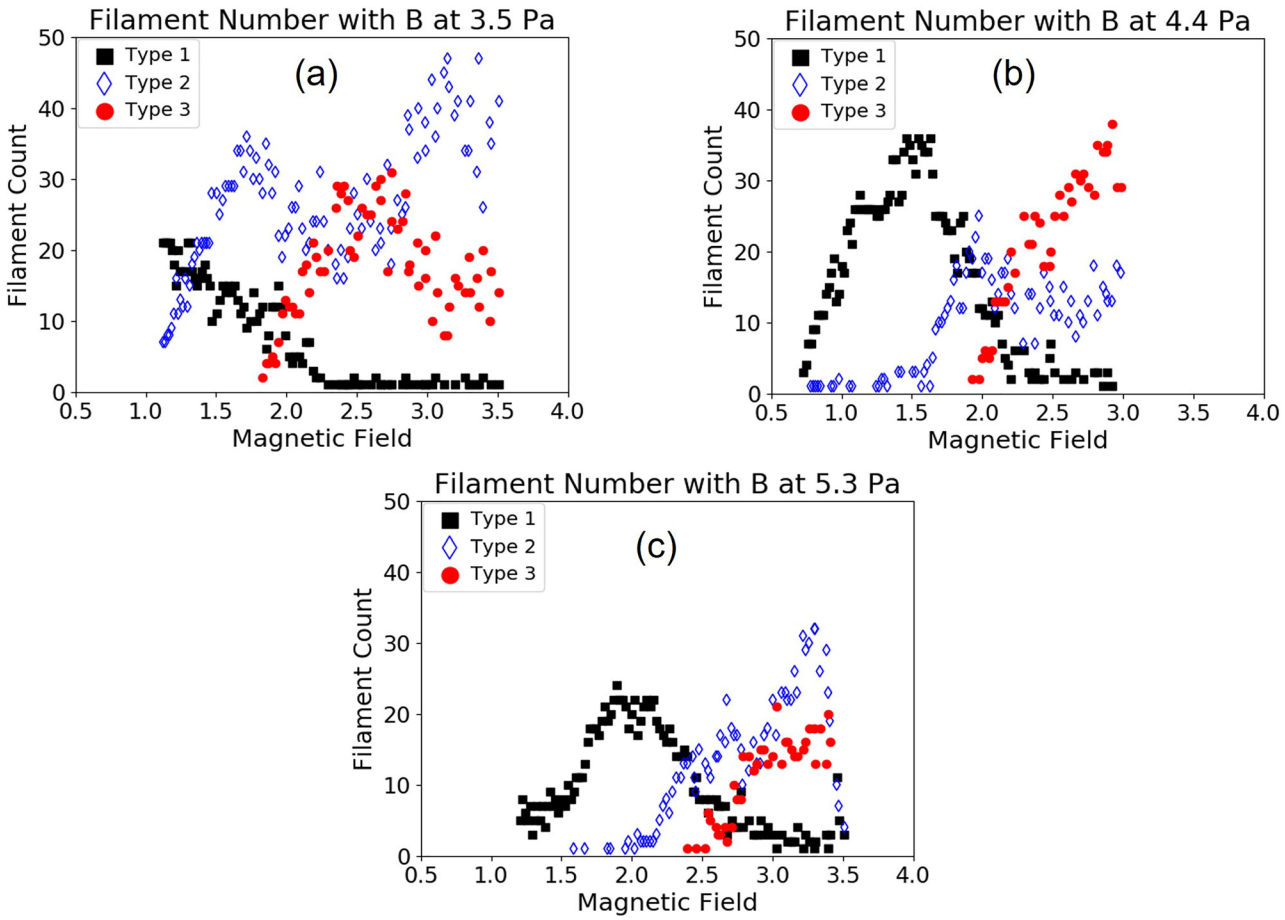

FIG. 7. Evolution of the observed plasma filaments with magnetic field. The "filament count" represents a larger occurrence of that type of filament. This representation shows that type 3 (spiral) appears at higher magnetic field, with a "turn-on" threshold that shifts to higher magnetic field ($B = \sim 1.8$ to ~ 2 to ~ 2.3 T) with increasing neutral pressure. A similar effect may be occurring with the type 2 (elongated) filaments. (a) $p = 3.5$ Pa, (b) $p = 4.4$ Pa, and (c) $p = 5.3$ Pa. In all cases, the type 1 (circular) filaments appear to have specific range of magnetic field over which they are present in the plasma and they dissipate at the higher magnetic field settings.

31 August 2023 11:57:18

Published under an exclusive license by AIP Publishing

that the filament formation is related to a competition between the electron transport, which is confined along the magnetic field lines, and the cross field ion transport. For example, in Ref. 15, the simulations show the formation of a spiral structure in the plasma. It is important to note that these simulations typically represent the initial formation of the filaments (for $\Delta t \leq 100\ \mu s$), but are not yet capable of representing the long-term, fluid-like ($\Delta t \sim 0.1$ s) evolution of the different filament morphologies. These limitations mean that we do not yet have a first-principles theoretical model to describe the underlying physical processes and this is the subject of ongoing experimental and computational work. Therefore, in the discussion of our experimental results, below, we will build upon the framework that has been developed by Menati *et al.* to determine if the experimental observations are qualitatively and quantitatively consistent.

The numerical results indicate that plasma filamentation occurs when the ion gyroradius is below the ion–neutral mean free path and the electron Debye length; i.e., $\rho_i \leq \lambda_{mfp}, \lambda_{De}$. For the experiments reported here, at pressures between $p = 0.67$ to 6.0 Pa in argon, under the assumption of room temperature neutral atoms and ions ($T_n = T_i = 0.025$ eV), this corresponds to ion-collision mean free paths, $\lambda_{mfp} = 1.8$ to 0.2 mm, respectively. Here, the collision cross section, that is used to compute the mean free path is $\sigma = 3.27 \times 10^{-18}$ m^2 as given in the papers by Hall and Thomas,[17] and Thomas and co-workers,[13] and based on the calculations by Khrapak.[18] When compared to the estimated ion gyroradii for argon atoms in the observational range from $B = 3.5$–1.0 T, the corresponding values are $\rho_i = 0.046$ mm to 0.16 mm, respectively. Therefore, on the basis of the first criterion that $\rho_i \leq \lambda_{mfp}$ in order for filaments to be observed in the plasma, we believe that the experimental results are consistent with that criterion.

For the second criterion, $\rho_i \leq \lambda_{De}$, this is more difficult to test because of the known challenges of operating Langmuir probes at high magnetic fields, particularly where the ion and electron gyroradii can be smaller than the diameter of the probe. From our previous $B = 0$ T experiments, the electron temperature in MDPX is reported as $T_e = 3.2 \pm 0.5$ eV and densities in the range $n \sim 0.4$–1.2×10^{15} m^{-3}. These parameters correspond to electron Debye lengths, $\lambda_{De} \sim 0.38$–0.66 mm. Again, this observation is generally consistent with the results from Menati. However, to further test this result, we analyzed the response of a single-tip Langmuir probe placed in the plasma over the range of pressure and magnetic fields investigated in this work. Although the initial probe traces were affected by the magnetic field, we were able to extrapolate some information from the data. The electron part of the Langmuir probe trace is generally considered unreliable because of a significant (> a factor of 20) distortion of the electron part of the current–voltage trace. However, the measurements suggest that the ion saturation current may provide some qualitatively useful information.

Figure 8 shows measurements of the average ion saturation current on a single tipped Langmuir probe that has a radius of r = 0.31 mm and a length of 8 mm, i.e., the average collected current for biases between $V_{probe} = -70$ and -50 V, for a neutral pressure range, $p = 2.4$–6.0 Pa (18–45 mTorr) and for magnetic fields from $B = 0$ T to $B = 1$ T. These measurements indicate that while there is a substantial drop in the ion saturation current between B = 0 T and B = 0.5 T (by about a factor of 8), the ion saturation does not vary significantly with increasing magnetic field, at least up to 1 T. One contributing factor to note is that between B = 0 T and B = 0.5 T, the ions

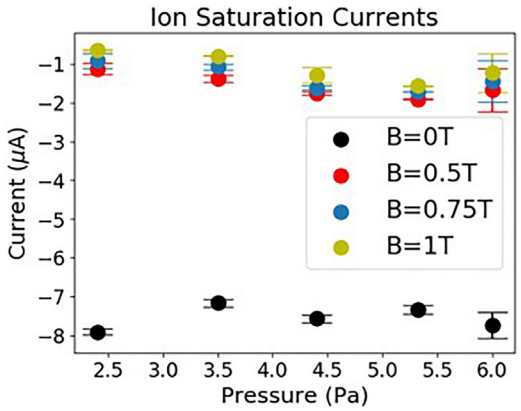

FIG. 8. Measured ion saturation current as a function of pressure and magnetic fields in MDPX at fixed RF power. While there is an initially large (∼ a factor of 8) drop of the ion saturation current between $B = 0$ T and $B = 0.5$ T, with increasing magnetic field, there is only a modest (< factor of 2) change in the ion saturation current between $B = 0.5$ T and $B = 1$ T. At $B = 0.5$ T, under the assumption of room temperature argon ions, the ion gyroradius is $\rho_i = 0.32$ mm which is smaller than the radius of the probe itself at, $r = 0.5$ mm. Therefore, the initial drop in ion saturation current may be attributable to a reduction in the effective collection area of the probe.

go from being unmagnetized with no gyroradius to having a gyroradius, $\rho_i = 0.32$ mm; this is comparable to the radius of the probe itself. This corresponds to a reduction in collection area from 15.6 mm^2 (total surface area) to a projected planar area of about 10 mm^2. Therefore, the observed initial drop in the ion saturation current may be attributable to the change in the effective ion collecting surface of the probe. However, a change in the electron temperature or a change in the plasma density could also contribute to this drop. Ultimately, the lack of a complete theoretical framework with which to properly describe the interpretation of a Langmuir probe trace at high magnetic field limits our ability to fully describe the response of the plasma with increasing magnetic field.

To expand beyond a basic comparison of the experimental observations with the model, it is noted that while magnetic field and pressure are useful parameters that can be easily modified in an experiment, they are closely coupled to each other through the definition of magnetization. In many works that discuss the application of magnetic fields to dusty plasmas, a parameter that is used to describe the "degree of magnetization" is the Hall parameter. The Hall parameter can be defined in term of characteristic frequencies or scale lengths for a collisional plasma and is given by $H_{ion} = \frac{\lambda_{mfp}}{2\pi\rho_i} \rightarrow H\left(\frac{B}{p}\right)$; where λ_{mfp} is the ion–neutral mean free path ($\sim 1/P$) and ρ_i is the gyroradius ($\sim 1/B$). In this definition, the factor of $2\pi\rho_i$ represents the effective circumference of the gyromotion so that $H_{ion} = 1$, is interpreted as an ion that completes a gyro-orbit before making a collision and is, therefore, the minimum criterion for defining when an ion (or any charged particle) becomes magnetized. The experiments described in this paper cover a range of magnetic fields and pressures and so the Hall parameter is a useful dimensionless quantity for describing the magnetization of the plasma.

The results presented in Fig. 9 show that there appears to be a threshold of magnetization at which each filament types appear. The

31 August 2023 11:57:18

Published under an exclusive license by AIP Publishing

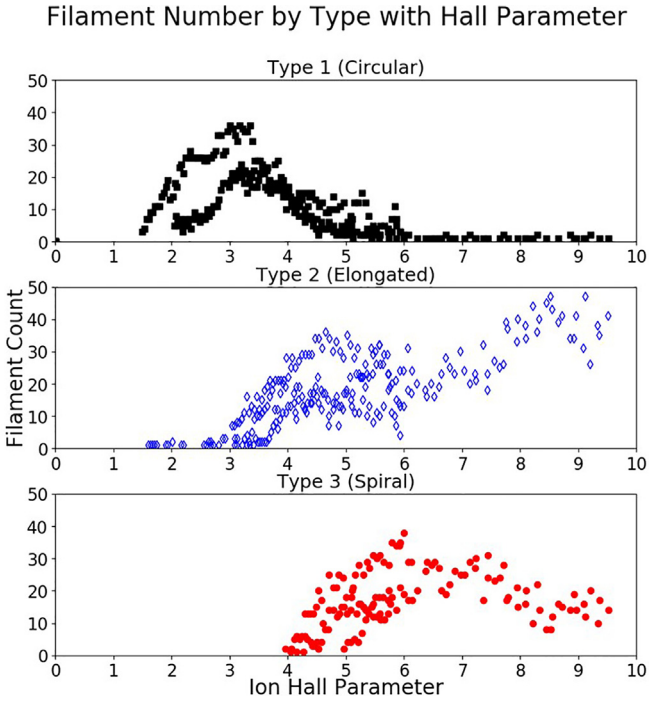

FIG. 9. Characteriztion of the filament type as a function of the ion Hall parameter using the data that is presented in Fig. 7. It is observed that, when comparing across the three pressures, 3.5, 4.4, and 5.3 Pa, with a scan over the magnetic field, there appears to be a very clear threshold for the appearance of each filament type. Additionally, as type 1 filament count decreases, type 2 and 3 filament count increases.

type 1 (circular) filaments begin to appear shortly after the ions become magnetized (as defined by $H_{ion} \geq 1$). An increasing ion magnetization appears to be required to observe first the type 2 (elongated), $H_{ion} \geq 3$, and type 3 (spiral), $H_{ion} \geq 4$. This result is new and unexpected, therefore future experimental and numerical studies will need to investigate the precise criteria in the plasma that lead to the formation of the different filament types and the processes that lead to their co-existence at specific values of the Hall parameter. At the present time, we do not have a formal theoretical framework from which to extrapolate the observed correlation between the degree of ion magnetization and the evolution in morphology of these filaments.

Another direction for future investigations is to expand our studies of filament behavior by characterizing filaments formed using different gases. This may provide additional opportunities to use a variety of diagnostic approaches, such as optical measurements (e.g., spectroscopy, laser induced fluorescence, or cavity ringdown spectroscopy) or *in situ* measurement (e.g., using dust particles as a diagnostic) to improve our characterization of the filaments as well as to confirm additional aspects of our simulation studies. We note that these are all speculative approaches that must be carefully evaluated to determine their potential use.

As a final comment, it is also noted that in these measurements, the filaments are being recorded as "fixed" objects in each image. When recorded at higher frame rates (>50 frames/second), it is observed that the filament types are not stable; i.e., some filaments can transform from one type of filament to another. This can sometimes occur periodically, e.g., an oscillation between a spiral (type 3) and an elongated (type 2) or by a single transformation. Additionally, individual filaments are observed to undergo a local rotation anywhere from ∼0.6 Hz to ∼1.4 Hz. The characterization of the dynamical behavior of the filaments is an ongoing activity and will be the subject of further discussion.

V. SUMMARY

This paper reports on observations and characterization of the spatial structure of plasma filaments with varying neutral gas pressure and magnetic field strength. Filamentation in magnetized plasmas has shown interesting results in self-organization and pattern formation; however, the shapes of individual columns can provide more insight into the formation and long-scale existence of these structures. They can also offer information into the physical mechanisms which contribute to their sustained presence at low neutral pressure and power conditions. The experimental conditions in which filaments are formed and such observations agree very well with those simulated and produced by Menati *et al.* allowing for a deeper investigation into the physics of filamentation. Additionally, experiments have confirmed the previously reported behavior of filamentary pattern formation but have also shown that there exists local dynamics on relatively smaller timescales compared to the filament existence. These dynamics will be investigated further in more detail. Finally, although additional experiments are necessary to confirm our assumptions, the observational data may suggest that the filaments follow azimuthal modal patterns. This evidence along with simulations may lead us to consider a fluid approach to future analysis.

ACKNOWLEDGMENTS

This work is supported by the U.S. Department of Energy, Grant No. DE-SC-0019176 and by the National Science Foundation EPSCoR program through Grant No. OIA-1655280. The construction of the MDPX device was funded through the NSF Major Research Instrumentation program, Grant No. PHY-1126067. The authors would also like to thank all the members of the Auburn University Magnetized Plasma Research Laboratory (MPRL) research team whose advice and suggestions have been invaluable in the pursuit of this project.

AUTHOR DECLARATIONS

Conflict of Interest

The authors have no conflicts to disclose.

DATA AVAILABILITY

The data that support the findings of this study are available from the corresponding author upon reasonable requrest.

REFERENCES

[1]E. Thomas, Jr., A. DuBois, B. Lynch, S. Adams, R. Fisher, D. Artis, S. LeBlanc, U. Konopka, R. L. Merlino, and M. Rosenburg, "Preliminary characteristics of magnetic field and plasma performance in the magnetized dusty plasma experiment (MDPX)," J. Plasma Phys. **80**(6), 803–808 (2014).

[2]U. Konopka, M. Schwabe, C. Knapek, M. Kretschmer, and G. Morfill, "Complex plasmas in strong magnetic field environments," AIP Conf. Proc. **799**, 181 (2005).

31 August 2023 11:57:18

Published under an exclusive license by AIP Publishing

[3]U. Konopka, P. Bandyopadhyay, D. Sharma, E. Thomas, and G. Morfill, "Circular, spiral, and point-like filamentation of a magnetized, radio frequency discharge," in *54th Annual Meeting of the APS Division of Plasma Physics, 29 October–2 November 2012* (American Physical Society, 2012).
[4]M. Schwabe, U. Konopka, P. Bandyopadhyay, and G. E. Morfill, "Pattern formation in a complex plasma in high magnetic fields," Phys. Rev. Lett. **106**, 215004 (2011).
[5]J. Chu and L. I, "Direct observation of Coulomb crystals and liquids in strongly coupled rf dusty plasmas," Phys. Rev. Lett. **72**, 4009 (1994).
[6]H. Thomas, G. Morfill, V. Demmel, J. Goree, B. Feuerbacher, and D. Möhlmann, "Plasma crystal: Coulomb crystallization in a dusty plasma," Phys. Rev. Lett. **73**, 652 (1994).
[7]O. Arp, D. Block, A. Piel, and A. Melzter, "Dust Coulomb balls: Three-dimensional plasma crystals," Phys. Rev. Lett. **93**, 165004 (2004).
[8]E. Thomas, Jr., U. Konopka, R. L. Merlino, and M. Rosenberg, "Initial measurements of two- and three-dimensional ordering, waves, and plasma filamentation in the magnetized dusty plasma experiment," Phys. Plasmas **23**, 055701 (2016).
[9]E. Thomas, Jr., B. Lynch, U. Konopka, M. Menati, S. Williams, R. L. Merlino, and M. Rosenberg, "Pattern formation in strongly magnetized plasmas: Observations from the magnetized dusty plasma experiment (MDPX) device," Plasma Phys. Controlled Fusion **62**, 014006 (2020).
[10]E. Thomas, Jr., R. L. Merlino, and M. Rosenberg, "Magnetized dusty plasmas: The next frontier for complex plasma research," Plasma Phys. Controlled Fusion **54**, 124034 (2012).
[11]E. Thomas, U. Konopka, D. Artis, B. Lynch, S. Leblanc, S. Adams, R. Merlino, and M. Rosenburg, "The magnetized dusty plasma experiment (MDPX)," J. Plasma Phys. **81**, 345810206 (2015).
[12]S. Jaiswal and E. Thomas, "Melting transition of two-dimensional complex plasma crystal in the DC glow discharge," Plasma Phys. Express **1**, 025014 (2019).
[13]T. Hall, E. Thomas, Jr., K. Avinash, R. Merlino, and M. Rosenberg, "Methods for the characterization of imposed, ordered structures in MDPX," Phys. Plasmas **25**, 103702 (2018).
[14]M. Menati, E. Thomas, and M. J. Kushner, "Filamentation of capacitively coupled plasmas in large magnetic fields," Phys. Plasmas **26**, 063515 (2019).
[15]M. Menati, B. Rasoolian, E. Thomas, and U. Konopka, "Experimental observation and numerical investigation of filamentary structures in magnetized plasmas," Phys. Plasmas **27**, 022101 (2020).
[16]J. Schindelin, I. Arganda-Carreras, E. Frise, V. Kaynig, M. Longair, T. Pietzsch, S. Preibisch, C. Rueden, S. Saalfeld, B. Schmid, J.-Y. Tinevez, D. J. White, V. Hartenstein, D. Eliceiri, P. Tomancak, and A. Cardona, "Fiji: An open-source platform for biological-image analysis," Nat. Methods **9**, 676 (2012).
[17]T. Hall and E. Thomas, "Dynamics of dust particles confined in imposed potential structures in strongly magnetized, low-temperature plasmas," Phys. Rev. E **102**, 023208 (2020).
[18]S. Khrapak, "Practical expression for an effective ion-neutral collision frequency in flowing plasmas of some noble gases," J. Plasma Phys. **79**, 1123 (2013).

31 August 2023 11:57:18

Published under an exclusive license by AIP Publishing